

# Influence of Water Amount on the Stability of Intercalated Vermiculites – Computational Study

EVA SCHOLTZOVÁ

Department of Theoretical Chemistry,  
Institute of Inorganic Chemistry, Slovak Academy of Sciences,  
Dúbravská cesta 9, 845 36 Bratislava,  
SLOVAKIA

**Abstract:** - Vermiculites are promising structures for synthesizing advanced materials applied in green chemistry. The *ab initio* density functional theory method and molecular dynamics were used to study the influence of water amount in the interlayer space of vermiculite intercalated by TMA cation on the stability of this hybrid structure, which can be used as a precursor. A detailed analysis of four model structures containing different amounts of water showed that the strength of hydrogen bonds between the TMA cation and vermiculite acting in the structure became weaker with the growing amount of water. The calculated vibrational spectra of respective structures confirmed this trend.

**Key-Words:** - TMA-vermiculite, water, DFT, modeling, interactions, wavenumbers, hydrogen bonds.

Received: July 23, 2024. Revised: January 26, 2025. Accepted: March 12, 2025. Published: April 10, 2025.

## 1 Introduction

Vermiculite is a clay mineral with a 2:1 type of layered structure, i.e., two tetrahedral sheets sandwiched with one octahedral sheet. Similarly, smectites (e.g., montmorillonite, beidellite, saponite) can be due to a cation-exchange reaction intercalated with organic cations, which help to improve the hydrophobic properties of clay minerals, which are typically hydrophilic. In the structures of clay minerals, various isomorphous substitutions are present in the tetrahedral (e.g.,  $\text{Si}^{4+}/\text{Al}^{3+}$ ,  $\text{Fe}^{3+}$ ) and octahedral (e.g.,  $\text{Al}^{3+}/\text{Mg}^{2+}$ ,  $\text{Fe}^{2+}$ ,  $\text{Mg}^{2+}/\text{Li}^{+}$ ) sheets, resulting in a residual negative charge of the layer of the structural unit. In vermiculite, the  $\text{Si}^{4+}/\text{Al}^{3+}$  substitutions predominate. This charge is counterbalanced by inorganic cations present in the interlayer space. Also, natural vermiculite contains charge-balancing inorganic cations such as  $\text{Na}^{+}$ ,  $\text{Ca}^{2+}$ , and/or  $\text{Mg}^{2+}$ , which are usually hydrated by water molecules in the interlayer space. These inorganic cations can be replaced by organic cations [1]. This process means inserting organic cations between the vermiculite layers, creating materials with unique and interesting properties. The intercalation of organic cation modifies vermiculite's physical and chemical characteristics, e.g., adsorption properties [2]. One of the most notable applications of organically modified vermiculites is in environmental remediation. These materials can effectively adsorb and immobilize pollutants, such as heavy metals and/or organic contaminants, from

water and soil. Furthermore, organo-vermiculites are used in catalysis as catalysts or supports in various chemical reactions. Vermiculites modified with organic cations thus can lead to the development of advanced materials for nanotechnology, electronics, and energy storage, for example [3]. These materials can create nanocomposites with enhanced e.g. mechanical and electrical properties, making them suitable for applications in sensors, batteries, and supercapacitors [4]. Modifying the structure of vermiculite changes its physicochemical properties and enables the creation of new materials with tailored properties for specific applications. The theoretical approach also used in the present work can bring additional information about the proposed structures, e.g., adequate characterization of the interactions between interlayer species and the surface of the clay minerals [5]. Using computational methods allows researchers to analyze the behavior of organic cations within the vermiculite structure by modeling and elucidating the mechanisms of intercalation and the resulting changes in material properties. Understanding the behavior of intercalated species in the interlayer space helps scientists to optimize the intercalation process to enhance the desired properties of the resulting materials [6]. Moreover, computational modeling can predict the stability and effectiveness of organically modified clay minerals under various conditions (e.g., chemical environment, temperature, and pressure [7]).

The present study aims to describe the interactions within the interlayer space of intercalated vermiculite (V) by tetramethylammonium cation (TMA). Generally, the water is present in the interlayer space of clays. Therefore, it is essential to know how varying amounts of water influence modified vermiculite's interactions and stability. This computational study can elucidate, at the atomic level, the running processes in the interlayer space when the water amount is growing. The smectites are often studied, but much information about vermiculites remains hidden. The novel information obtained by modeling is crucial because the changes in the interactions can also impact other physicochemical properties, e.g., the vibrations of functional groups involved in interactions with additional water molecules in the interlayer space of vermiculite. Such a detailed study has not yet been carried out for modified vermiculite at this level of theory.

## 2 Problem Formulation

### 2.1 Model Preparation

An essential thing in preparing the structural models is considering the compromise between the realistic structure and size of the computational model to have achievable computational demand. The strategy was the following: The structure of vermiculite that is close to reality (experiment) is appreciated for studying the changes in the interlayer space. This work used the experimental structure of TMAV [2] as a starting point. As the authors expected, two TMA cations were present in the interlayer space instead of four, forming the stable structure in the elementary cell. The lattice parameters of the computational cell were identical to the published lattice parameters  $a=5.353(1)$ ,  $b=9.273(2)$ ,  $c=13.616(6)$  Å and  $\beta=97.68^\circ$  (space group  $C2/m$ ) in the experimental work. The model was labeled as 0W and had half occupied the positions of TMA cations. Further models with different amounts of water were prepared to study the influence of water on the mutual interactions in the interlayer space of the TMAV: 2W model – in which two water molecules were placed at the vacant positions of the other two TMA cations. The computational cell of the 2W model was enlarged to  $2a1b1c$  to study the influence of the larger amount of water. The enlarged models contained four TMA cations and four molecules of water. Since one TMA cation has the same volume as three water molecules, the substitution of one TMA cation by three water molecules was done (7W model). By

substituting the second TMA cation, the 10W model was proposed.

### 2.2 Computational Details

The calculations using the DFT method implemented in the Vienna *Ab Initio* Simulation Package (VASP) program were done [8], [9]. The exchange-correlation energy was expressed in the framework of the generalized gradient approximation (GGA) using the PBE functional [10]. The Kohn-Sham equations were solved using the variational method in a plane-wave (PW) basis set with an energy cut-off of 500 eV. The electron-ion interactions were described using the projector-augmented-wave (PAW) method [11], [12]. Brillouin-zone sampling was restricted to the  $\Gamma$ -point due to the large computational cells. All calculations were performed with the experimental cell parameters, and all the atomic coordinates were allowed to vary. The relaxation criteria were  $10^{-5}$  eV/atom for the total energy change and 0.005 eV/Å for the maximum force acting on any atom. It should be mentioned that the method has some limitations, e.g., overestimating the electron delocalization and underestimation dispersion interactions. However, the dispersion interactions acting in the interlayer space were corrected within the D3-scheme [13] implemented in the VASP 5.4. version. It is one of the techniques that improves the final results. Except for the D2-D4 correction methods, e.g., the van der Waals technique exists. However, this method is highly computationally demanding for the present systems. Since the flexible water molecules were present in the interlayer space, the ab initio molecular dynamics simulations were applied. Owing to the computational demands of AIMD, the energy cut-off was reduced to 400 eV, and the required convergence in total energy to  $10^{-4}$  eV. The Verlet velocity algorithm [14] with a time step of 1 fs was chosen for a numerical solution of equations of motion. First, the finite temperature calculations were performed on a canonical (*NVT*) ensemble applying the Nosé Hoover thermostat procedure [15] at the simulation temperature of 300 K to equilibrate the structure and use the MD length of 5 ps. Then, the system was changed to the microcanonical (*NVE*) ensemble to obtain the vibrational density of states, VDOS (in other words, power spectra). In this case, the total length of the MD run was ten ps. The results of the AIMD calculations were interpreted in a wavenumber domain by calculating the Fourier transform of the velocity autocorrelation functions to obtain VDOS.

### 3 Problem Solution

After calculations, the proposed models were analyzed in detail. The electrostatic and dispersion interactions and hydrogen bonds are present in the examined structures. The focus was given to hydrogen bonds because they are essential for the stability of the hybrid structures of organic surfactant-clay minerals.

#### 3.1 Hydrogen Bond Analysis

The analysis of hydrogen bonds was done according to the criteria published in [16], and in the discussion, the focus was on the H...Acceptor (min, median, max values) for respective hydrogen bonds acting in the studied structures (Table 1).

Table 1. H...A hydrogen bonds – min, median, max in [Å] in the examined structures

Models TMA-V	H...A
<b>C-H...O<sub>basal</sub></b>	
0w	1.92; <u>2.11</u> ; 2.54
2w	2.05; <u>2.29</u> ; 2.55
7w	1.98; <u>2.31</u> ; 2.56
10w	2.04; <u>2.38</u> ; 2.58
<b>C-H...O<sub>water</sub></b>	
0w	-
2w	1.98; <u>2.01</u> ; 2.30
7w	2.01; <u>2.35</u> ; 2.59
10w	2.08; <u>2.43</u> ; 2.45
<b>O-H<sub>water</sub>...O<sub>basal</sub></b>	
0w	-
2w	1.55; <u>1.67</u> ; 2.57
7w	1.58; <u>1.79</u> ; 2.37
10w	1.58; <u>1.99</u> ; 2.52
<b>O-H<sub>water</sub>...O<sub>water</sub></b>	
0w	-
2w	-
7w	1.78; <u>1.90</u> ; 2.58
10w	1.56; <u>2.14</u> ; 2.58
<b>O-H<sub>inner</sub>...O<sub>water</sub></b>	
0w	-
2w	2.16; 2.46
7w	1.60; 1.70; 1.76
10w	1.71; 1.86
<b>O-H<sub>inner</sub>...O<sub>basal</sub> intra</b>	
0w	-
2w	-
7w	2.45; 2.57
10w	2.56

The structures showed that in the interlayer space of the TMA-vermiculite models exist two types of C-H...O hydrogen bonds (C-H...O<sub>basal</sub>) corresponding to cation-clay interactions, and C-H...O<sub>water</sub> corresponding to cation-water interaction), and two types of the O-H...O hydrogen bonds: O-H<sub>water</sub>...O<sub>basal</sub> representing strong to moderate water-clay interactions, and weaker O-H<sub>water</sub>...O<sub>water</sub> representing water-water interactions.

Moreover, in the models of TMA-vermiculite with water, moderate hydrogen bonds of the O-H<sub>inner</sub>...O<sub>water</sub> type are present. With the growing amount of water, the O-H<sub>inner</sub>...O<sub>basal</sub> of weak strength also appeared. The C-H...O<sub>water</sub> hydrogen bonds are stronger than C-H...O<sub>basal</sub> and the O-H<sub>water</sub>...O<sub>water</sub> hydrogen bonds are weaker than O-H<sub>water</sub>...O<sub>basal</sub> (Table 1, Fig. 1, Fig. 2, Fig. 3 and Fig. 4).

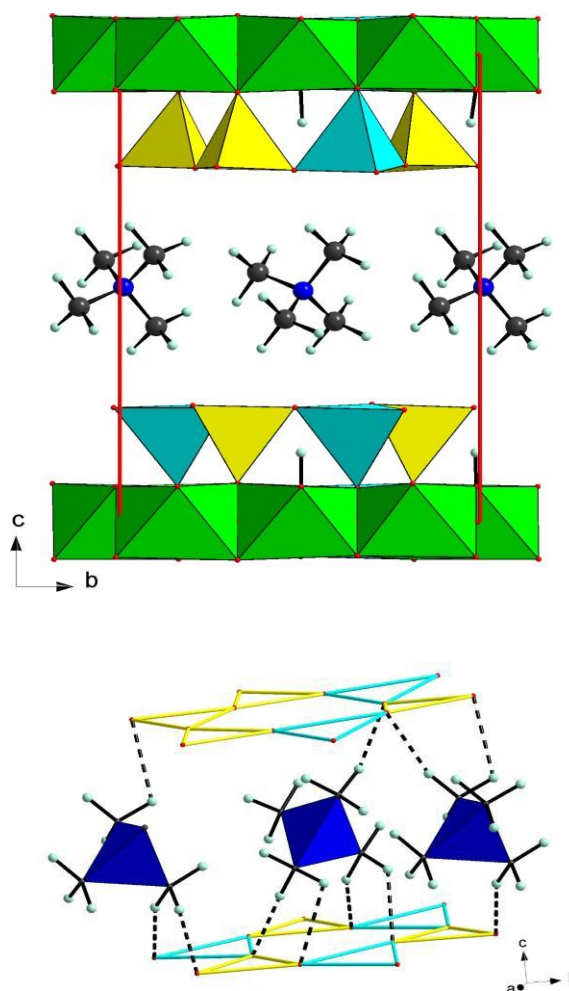


Fig. 1: Optimized 0W model (up), C-H...O<sub>basal</sub> hydrogen bonds in the interlayer space of 0W structure (bottom). The tetrahedral sheet is illustrated just as a siloxane surface for clarity.

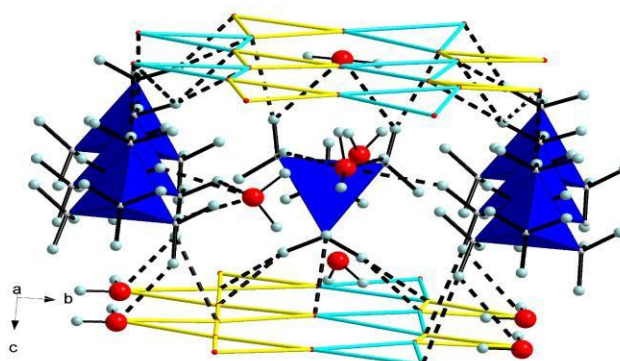
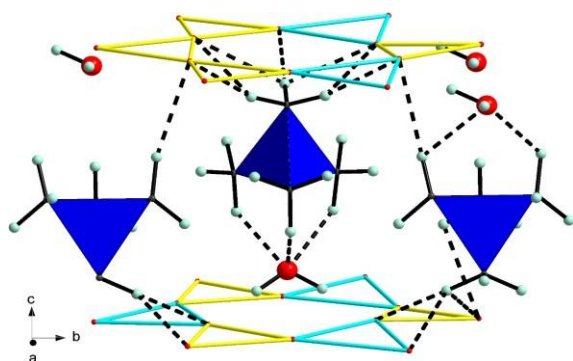
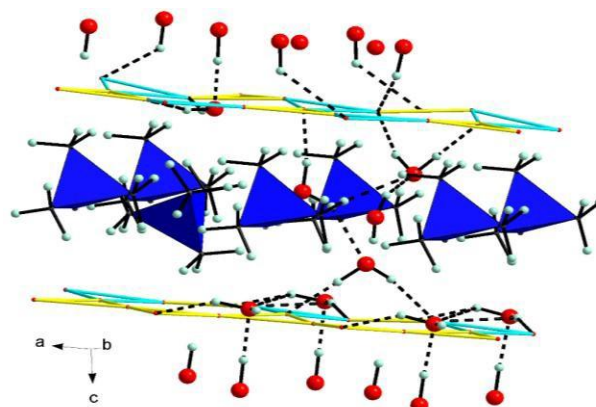
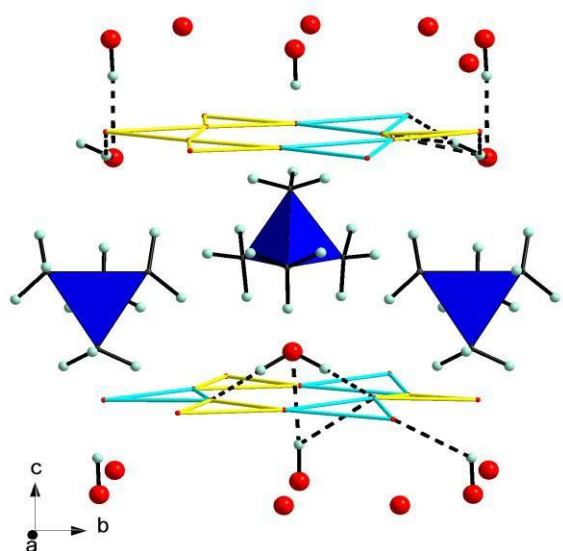
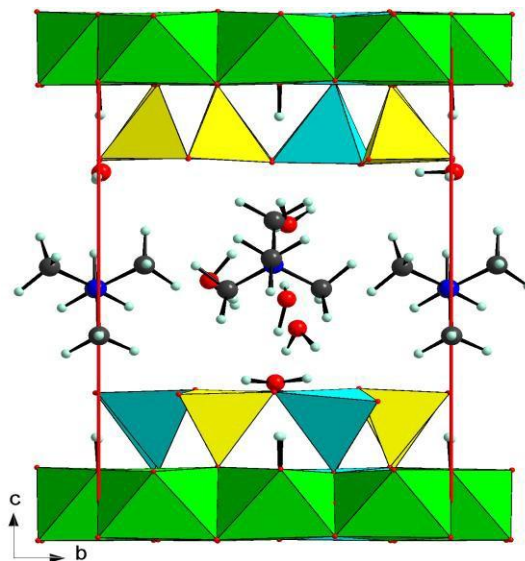
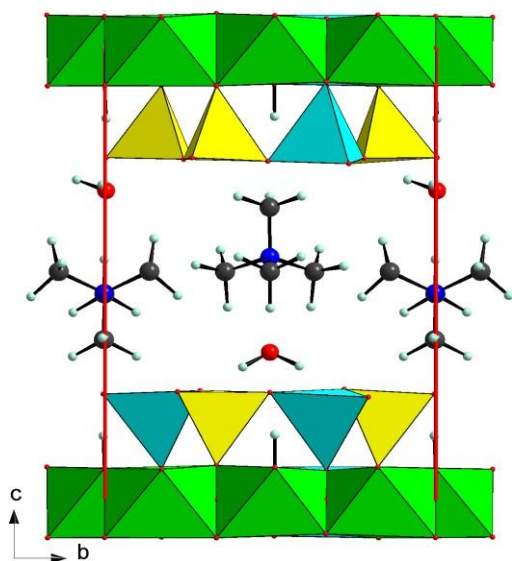


Fig. 2: Optimized 2W model (up),  $O-H_{\text{water}} \cdots O_{\text{basal}}$  and  $O-H_{\text{inner}} \cdots O_{\text{water}}$  hydrogen bonds (middle) and  $C-H \cdots O_{\text{basal}}$  and  $C-H \cdots O_{\text{water}}$  hydrogen bonds (bottom) in the interlayer space of 2W structure. For clarity, the tetrahedral sheet is illustrated just as a siloxane surface, and only the  $O-H_{\text{inner}}$  groups are present on the octahedral sheet.

Fig. 3: Optimized 7W model (up),  $O-H_{\text{water}} \cdots O_{\text{basal}}$ ,  $O-H_{\text{water}} \cdots O_{\text{water}}$ ,  $O-H_{\text{inner}} \cdots O_{\text{basal}}$  intra and  $O-H_{\text{inner}} \cdots O_{\text{water}}$  hydrogen bonds (middle) and  $C-H \cdots O_{\text{basal}}$  and  $C-H \cdots O_{\text{water}}$  hydrogen bonds (bottom) in the interlayer space of 7W structure. For clarity, the tetrahedral sheet is illustrated as a siloxane surface, and only the  $O-H_{\text{inner}}$  groups are present on the octahedral sheet.

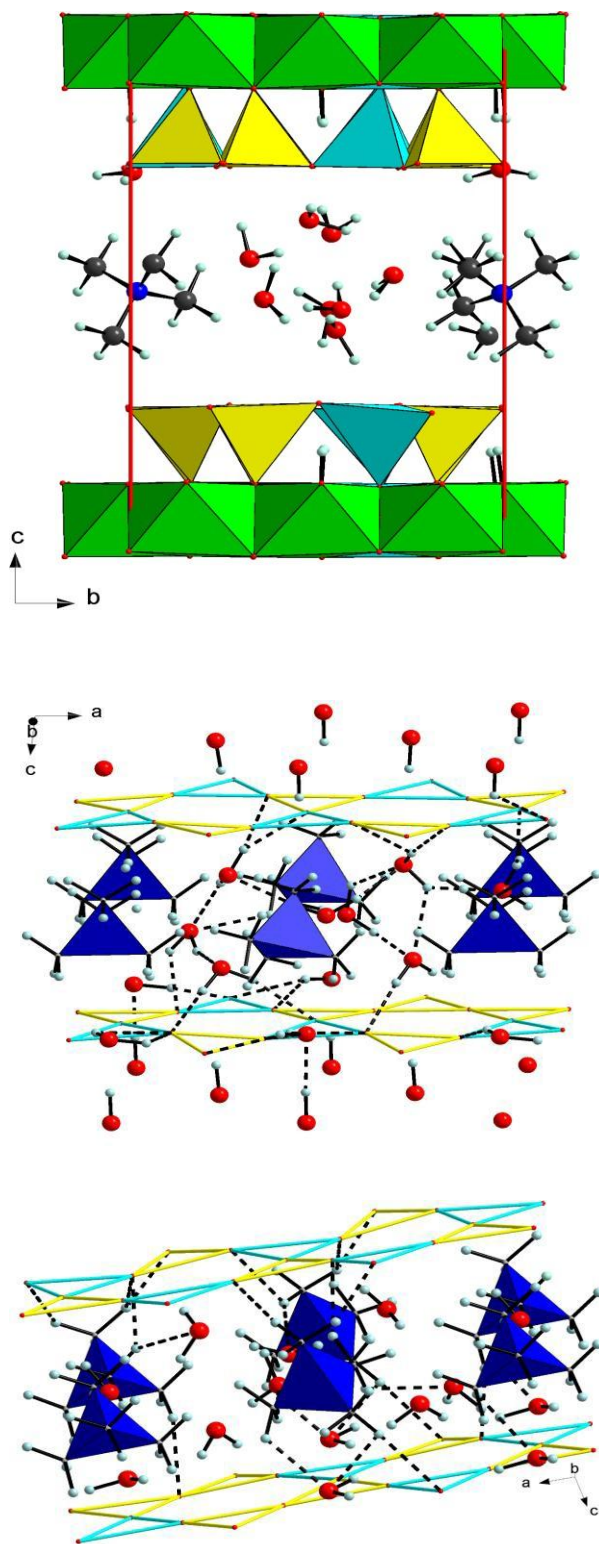


Fig. 4: Optimized 10W model (up),  $O-H_{\text{water}} \cdots O_{\text{basal}}$ ,  $O-H_{\text{water}} \cdots O_{\text{water}}$ ,  $O-H_{\text{inner}} \cdots O_{\text{basal}}$  intra and  $O-H_{\text{inner}} \cdots O_{\text{water}}$  hydrogen bonds (middle) and  $C-H \cdots O_{\text{basal}}$  and  $C-H \cdots O_{\text{water}}$  hydrogen bonds (bottom) in the interlayer space of 10W structure. For clarity, the tetrahedral sheet is illustrated as a siloxane surface, and only the  $O-H_{\text{inner}}$  groups are present on the octahedral sheet.

The  $C-H \cdots O_{\text{basal}}$  hydrogen bonds responsible for direct interaction with the vermiculite siloxane surface become weaker with the growing amount of water. The increasing amount of water tends to group, forming a 'zeolitic water' type of structure [17] (Figure 4).

### 3.2 Vibrational Spectra

The total density of states for the respective proposed structures was calculated and analyzed (Figure 5). It should be mentioned that calculated wavenumber values are overestimated because of the DFT method compared with experimental values.

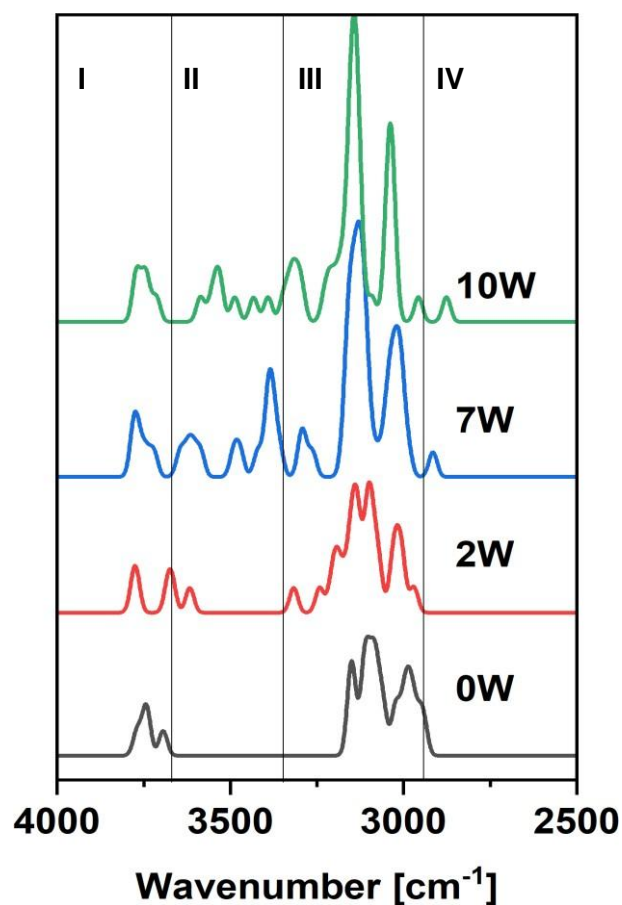


Fig. 5: Calculated vibrational spectra for modelled structures of intercalated vermiculites. I –  $OH_{\text{inner}}$  stretchings, II –  $OH_{\text{water}}$  stretchings, III – CH stretchings and IV –  $OH_{\text{water}}$  stretchings involved in hydrogen bonds.

Despite this, calculations provide a valuable analysis of trends in the spectra, and the respective vibrations can be recognized. The stretching vibrations of OH and CH groups were analyzed in detail due to the visible changes in the position of the characteristic bands of the respective vibrations.

The highest energy bands (4000 - 3680  $\text{cm}^{-1}$ ) represent the first region of the stretching vibrations of the inner hydroxyl groups in the vermiculite structure and changes in the position of these bands are influenced minimally by the presence of the intra-hydrogen bonds and interactions with the water molecules in 7W and 10W model structures. This vibration was detected in the experimental IR spectrum at 3723  $\text{cm}^{-1}$  for the  $\text{Mg}_3\text{OH}$  group and 3670  $\text{cm}^{-1}$  for  $\text{Mg}_2\text{AlOH}$  one [18].

The second region (3680-3300  $\text{cm}^{-1}$ ) is formed by the stretching vibrations of the water OH hydroxyl groups (exp. 3300  $\text{cm}^{-1}$  [18]). The more structured bands appear for the structures with the higher amount of water. In the third region (3300 – 2850  $\text{cm}^{-1}$ ), the CH stretching vibrations act (exp. 2915 – 2846  $\text{cm}^{-1}$  [18]), and the blueshift with the growing amount of water is visible. The blueshift is induced by the involvement of the CH groups in the hydrogen bonds and caused by  $sp^3$  hybridization [19]. The stretching vibrations of the OH groups involved in the hydrogen bonds are present in the fourth discussed region (2850 – 2500  $\text{cm}^{-1}$ ). The redshift in the band positions with the growing amount of water is apparent. In all the regions, the asymmetric stretching vibrations had a higher energy value than the symmetric ones [20].

Figure 6 shows the relation between the wavenumber of the strongest  $\text{O-H}_{\text{water}} \cdots \text{O}_{\text{basal}}$  hydrogen bond present in the respective structures as an example to quantify the shifts in bands of the vibrational spectra at growing amounts of water.

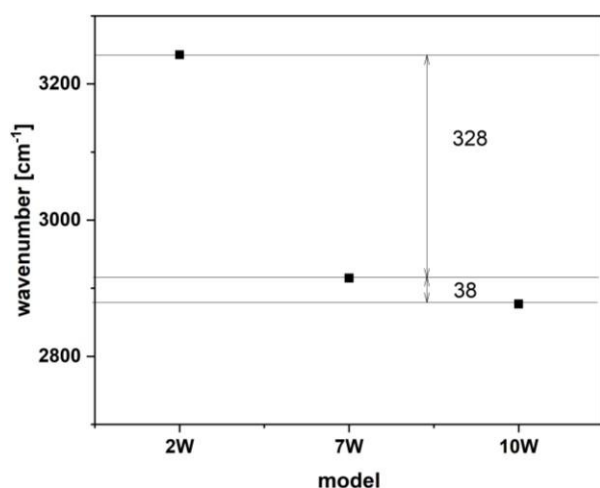


Fig. 6: The redshift in the wavenumbers of the OH groups involved in the  $\text{O-H}_{\text{water}} \cdots \text{O}_{\text{basal}}$  hydrogen bond is quantified.

The additional water in the 7W model caused a significant redshift (328  $\text{cm}^{-1}$ ) in the spectrum,

reflecting the fixation of respective water molecules by additional hydrogen bonds arising from the larger amount of water molecules. A further amount of water in the 10W model shifted the wavenumber by an additional 38  $\text{cm}^{-1}$ . This analysis confirmed the relationship between the strength of hydrogen bonds in the structures and the amount of structural water.

## 4 Conclusion

The present study analyzed the most important interactions among the interlayer species in all calculated model structures of intercalated vermiculite by TMA cation. The hydrogen bonds by which the TMA cation interacts with the siloxane surface of vermiculite became weaker with the growing amount of water in the studied model structures of TMAV.

Detailed analysis of the interactions' behavior revealed the negative impact of the growing amount of water on the stability of the modified vermiculite by organic surfactant, which can be used as a precursor in the synthesis of advanced materials based on clay minerals.

The weaker interactions of the TMA cation with the siloxane surface of vermiculite also confirmed vibrational spectra, which showed a present redshift in the OH vibrations and blueshift in the CH vibrations of these functional groups involved in the hydrogen bonds in the interlayer space and with the skeleton of vermiculite.

Since vermiculite forms stable structures with TMA cation, it can be used for further applications in green technologies. Its stability is higher with a lower amount of water present in the interlayer space. These findings were obtained for 300 K; others, e.g., thermal and mechanical stability, remain unknown. Thus, after these pilot examinations, further testing is required.

### Acknowledgement:

Funded by the EU NextGenerationEU through the Recovery and Resilience Plan for Slovakia under project No. 09I03-03-V04-00009.

### Declaration of Generative AI and AI-assisted Technologies in the Writing Process

During the preparation of this work, the author used Grammarly in order to check grammar and spelling. After using this tool/service, the author reviewed and edited the content as needed and takes full responsibility for the content of the publication.

References:

- [1] X. X. Huo, L. M. Wu, L. B. Liao, Z. G. Xia, L. J. Wang, The effect of interlayer cations on the expansion of vermiculite. *Powder Technology*, Vol.224, 2012, pp. 241-246. DOI: [10.1016/j.powtec.2012.02.059](https://doi.org/10.1016/j.powtec.2012.02.059)
- [2] A. Vahedi-Faridi, S. Guggenheim, Crystal structure of tetramethylammonium-exchanged vermiculite. *Clays and Clay Minerals*, Vol.45, No.6, 1997, pp. 859-866. DOI: [10.1346/CCMN.1997.0450610](https://doi.org/10.1346/CCMN.1997.0450610)
- [3] M. Marosz, A. Kowalczyk, L. Chmielarz, Modified vermiculites as effective catalysts for dehydration of methanol and ethanol. *Catalysis Today*, Vol.355, 2020, pp. 466-475. DOI: [10.1016/j.cattod.2019.07.003](https://doi.org/10.1016/j.cattod.2019.07.003)
- [4] X. X. Wang, P. Z. Wang, W. L. Tian, H. L. Bu, K. W. Zhang, Smart Energy Clays: Chemical Vapor Deposition of PEDOT in Expanded Vermiculite Blocks for Electrochemical Energy Storage. *ACS Sustainable Chemistry & Engineering*, Vol.11, No.49, 2023, pp. 17510-17518. DOI: [10.1021/acssuschemeng.3c05695](https://doi.org/10.1021/acssuschemeng.3c05695)
- [5] C.T. Johnston, Probing the nanoscale architecture of clay minerals. *Clay Minerals*, Vol.45, No.3, 2010, 245-279. DOI: [10.1180/claymin.2010.045.3.245](https://doi.org/10.1180/claymin.2010.045.3.245)
- [6] K. S. Katti, D. Sikdar, D. R. Katti, P. Ghosh, D. Verma, Molecular interactions in intercalated organically modified clay and clay-polycaprolactam nanocomposites: Experiments and modeling. *Polymer*, Vol.47, No.1, 2006, pp. 403-414. DOI: [10.1016/j.polymer.2005.11.055](https://doi.org/10.1016/j.polymer.2005.11.055)
- [7] M. A. Zaeem, S. Thomas, S. Kavousi, N. Zhang, T. Mukhopadhyay, A. Mahata, Multiscale computational modeling techniques in study and design of 2D materials: recent advances, challenges, and opportunities. *2D Materials*, Vol.11, No.4, 2024, Article 042004. DOI: [10.1088/2053-1583/ad63b6](https://doi.org/10.1088/2053-1583/ad63b6)
- [8] G. Kresse, J. Hafner, Ab-initio molecular-dynamics for open-shell transition-metals. *Physical Review B*, Vol.48, 1993, pp. 13115-131180. DOI: [10.1103/PhysRevB.48.13115](https://doi.org/10.1103/PhysRevB.48.13115)
- [9] G. Kresse, J. Furthmuller, Efficient iterative schemes for ab initio total-energy calculations using a plane-wave basis set. *Physical Review B*, Vol.54, No.16, 1996, pp. 11169-11186. DOI: [10.1103/PhysRevB.54.11169](https://doi.org/10.1103/PhysRevB.54.11169)
- [10] J.P. Perdew, K. Burke, Y. Wang, Generalized gradient approximation for the exchange-correlation hole of a many-electron system, *Physical Review B*, Vol.54, No.23, 1996, pp. 16533-16539. DOI: [10.1103/PhysRevB.54.16533](https://doi.org/10.1103/PhysRevB.54.16533)
- [11] P.E. Blochl, Projector augmented-wave method, *Physical Review B*, Vol.50, No.24, 1994, pp. 17953-17979. DOI: [10.1103/PhysRevB.50.17953](https://doi.org/10.1103/PhysRevB.50.17953)
- [12] G. Kresse, D. Joubert, From ultrasoft pseudopotentials to the projector augmented-wave method. *Physical Review B*, Vol.59, No.3, 1999, pp. 1758-1775. DOI: [10.1103/PhysRevB.59.1758](https://doi.org/10.1103/PhysRevB.59.1758)
- [13] S. Grimme, J. Antony, S. Ehrlich, H. Krieg, A consistent and accurate ab initio parametrization of density functional dispersion correction (DFT-D) for the 94 elements H-Pu. *Journal of Chemical Physics*, Vol.132, No.15, 2010, Article 154104. DOI: [10.1063/1.3382344](https://doi.org/10.1063/1.3382344)
- [14] M. Ferrario, J.P.P. Ryckaert, Constant pressure-constant temperature molecular-dynamics for rigid and partially rigid molecular-systems. *Molecular Physics*, Vol.54, No.3, 1985, pp. 587-603. DOI: [10.1080/00268978500100451](https://doi.org/10.1080/00268978500100451)
- [15] S. Nose, A unified formulation of the constant temperature molecular-dynamics methods. *Journal of Chemical Physics*, Vol.81, No.1, 1984, pp. 511-519. DOI: [10.1063/1.447334](https://doi.org/10.1063/1.447334)
- [16] G. Desiraju, T. Steiner, The Weak Hydrogen Bond in Structural Chemistry and Biology. *Oxford University Press, Oxford, UK.*, 2006. 2nd edition. DOI: [10.1021/cg0100078](https://doi.org/10.1021/cg0100078)
- [17] I.E. Grey, A.R. Kampf, Zeolitic water in strunzite-group minerals. *Mineralogical Magazine*, Vol.82, No.2, 2018, pp. 291-299.
- [18] A. Vimond-Laboudigue, Prost, R., Etude comparee des complexes hectorite- et vermiculite-decylammonium a l'aide des spectrometries infrarouge et raman. *Clay Minerals*, Vol.30, No.4, 1995, pp. 337-352. DOI: [10.1180/claymin.1995.030.4.07](https://doi.org/10.1180/claymin.1995.030.4.07)
- [19] E. Scholtzova, D. Tunega, J. Madejova, H. Palkova, Theoretical and experimental study of montmorillonite intercalated with tetramethylammonium cation. *Vibrational Spectroscopy*, Vol.66, 2013, pp. 123-131. DOI: [10.1016/j.vibspec.2013.02.006](https://doi.org/10.1016/j.vibspec.2013.02.006)
- [20] E. Scholtzova, Insight into the Structure of TMA-Hectorite: A Theoretical Approach. *Minerals*, Vol.11, No.5, 2021, Article 505. DOI: [10.3390/min11050505](https://doi.org/10.3390/min11050505)

**Contribution of Individual Authors to the Creation of a Scientific Article (Ghostwriting Policy)**

The author contributed in the present research, at all stages from the formulation of the problem to the final findings and solution.

**Sources of Funding for Research Presented in a Scientific Article or Scientific Article Itself**

Funded by the EU NextGenerationEU through the Recovery and Resilience Plan for Slovakia under the project No. 09I03-03-V04-00009.

**Conflict of Interest**

The author has no conflict of interest to declare that is relevant to the content of this article.

**Creative Commons Attribution License 4.0 (Attribution 4.0 International, CC BY 4.0)**

This article is published under the terms of the Creative Commons Attribution License 4.0

[https://creativecommons.org/licenses/by/4.0/deed.en\\_US](https://creativecommons.org/licenses/by/4.0/deed.en_US)